Expanded use of a fast photography technique to characterize laser-induced plasma plumes

M. A. Valverde–Alva[a], T. García-Fernández[b], G. Diáz-Cortés[a], J. L. Sánchez-Llamazares[c], E. Rodríguez-González[d], C. Sánchez-Aké[e], A. Quintana-Nedelcos[c], and M. Villagrán-Muniz[e]

[a]*Posgrado en Ciencia e Ingeniería de Materiales, Universidad Nacional Autónoma de México, México D.F., C.P. 04510, México.*

[b]*Universidad Autónoma de la Ciudad de México, Prolongación San Isidro 151, San Lorenzo Tezonco, México D.F., 09790, México. e-mail: tupacgarcia@yahoo.com*

[c]*Instituto Potosino de Investigación Científica y Tecnológica A.C., Camino a la Presa San José 2055 Col. Lomas 4[a], S.L.P. 78216, San Luis Potosí, México.*

[d]*CICATA-IPN Unidad Altamira. Tamaulipas, México.*

[e]*CCADET Universidad Nacional Autónoma de México, México D.F., 04510, México.*

Received 26 August 2013; accepted 26 February 2014

Expanded use of fast photography is proposed to characterize laser ablation plasma plumes by the analysis of a set of photographs by means of appropriate mathematical algorithms. The laser ablation plasma plumes studied were generated by ablation of both a multicomponent target of the nominal composition $Ni_{50}Mn_{37}Sn_{13}$ and a highly pure Cu target (Cu) using a Q-switched Nd-YAG laser system.The experiments were conducted under different background argon pressures. Several photograph parameters such as intensity per unit time of exposure for a pixel, mean intensity per pixel per unit time of exposure, integrated intensity and cross correlation were studied. The intensity per unit time of exposure allowed for identification of the fast component of the triple structure of the expanding plasma into the background gas (that travels at a speed close to the one measured in vacuum). This parameter together with the use of cross correlation enabled the identification of regions of the expanded plasma plume with higher and lower similarities in their optical emission behavior. The mean intensity per pixel per unit time of exposure can be used as a measurement of the amount of light emitted by the plume as a function of time.

Keywords: Plasma diagnostics; laser ablation; digital image processing; fast photography; plasma plume splitting.

PACS: 52.38.Mf; 07.05.Pj; 52.70-m

1. Introduction

Fast photography of laser-induced plasma optical emission by means of a nanosecond gated intensified charged coupled device (ICCD) is a valuable way to acquire information on the local structure, constituent particle dynamics and laser ablated plasma plume geometry [1]. Using this technique one can observe the two-dimensional evolution of the ablation plume optical emission that expands three dimensionally. Previously, this procedure has been used to create position-versus-time plots of the plasma plume expansion front [2,3], as well as to study the influence of processing parameters during deposition of thin films by laser ablation on the plasma plume behavior such as background gas pressure [2,4,5] and laser energies [6]. By means of the fast photography technique several phenomena such as plume splitting, plume sharpening, and plume speed reduction [2-5,7] can be studied. The slowing-down and attenuation dynamics of laser ablation plasma plumes at intermediate values of background gas atmosphere during deposition are processes of significant interest for thin film growth by the pulsed-laser deposition (PLD) technique since the density and kinetic energy of the species that arrive to the substrate are key deposition parameters [8]. It has been demonstrated that the structure and morphology of the films grown by PLD are highly dependent on the kinetic energy of species existing in the plasma plume [9,10]. Several researches have observed plasma plume splitting using a fast photography technique during laser ablation at intermediate-pressure background gases [2,3,11,12]. In these cases splitting consists of the existence of two distinct luminous sectors under a background pressure where strong optical emission is observed due to particle collision both in the plume body (the slower moving/stationary component near the target surface) and the plume expansion front [12]. Using space- and time-resolved spectral emission and Langmuir probe techniques other authors have reported the appearance of a third fast component expanding through the background gas with a vacuum-like constant velocity [2,13]. However, previous fast photography research was not enough for the accurate determination of this triple structure formed during laser ablation in intermediate-background gas pressures. In this work, we analyze the laser-induced plasma plumes originating from both a multicomponent target of nominal composition $Ni_{50}Mn_{37}Sn_{13}$ and a single-element Cu-target through the extended use of fast photography. Several photograph parameters such as intensity per unit time of exposure for a pixel, mean intensity per pixel per unit time of exposure, in-

tegrated intensity and cross correlation were used to describe some characteristics of the ablation plume.

2. Experimental Procedure

2.1. Experimental set-up for laser ablation plasma plume analysis using fast photography

The laser ablation experimental setup used for the experiments is shown in Fig. 1. The system uses a Continuum Q-switched Nd-YAG laser system, model Surelite I with $\lambda = 1064$ nm, E = 100 mJ/pulse, $f = 1$ Hz, fluence of 12 J/cm^2 and pulse duration of 8 ns. The pulsed laser beam is focused on the rotating target by means of a spherical lens having a 25-cm focal length. A 45-degree-angle laser beam incidence with respect to the target surface was maintained. The two cylindrical targets used for the study were as follows: (a) a disc of 1.0 cm in diameter and 0.5 cm thickness with the nominal composition $Ni_{50}Mn_{37}Sn_{13}$, previously produced by argon arc melting from highly pure elements (99.98% pure Ni, 99.98% pure Mn, and 99.99 % pure Sn); and (b) a disc of 1.0 cm in diameter and 0.6 cm thickness of 99.99 % pure Cu.

In order to study the influence of pressure on the plasma expansion dynamics, the background argon pressure was varied from 10^{-5} Torr (vacuum) to 0.694 Torr. The pressure in the chamber was established by accurately controlling both the argon flux injection (99.99% pure argon) and the exhaust rate by using an integrated multigas controller coupled to the vacuum system (model 647 C, from MKS Instruments).

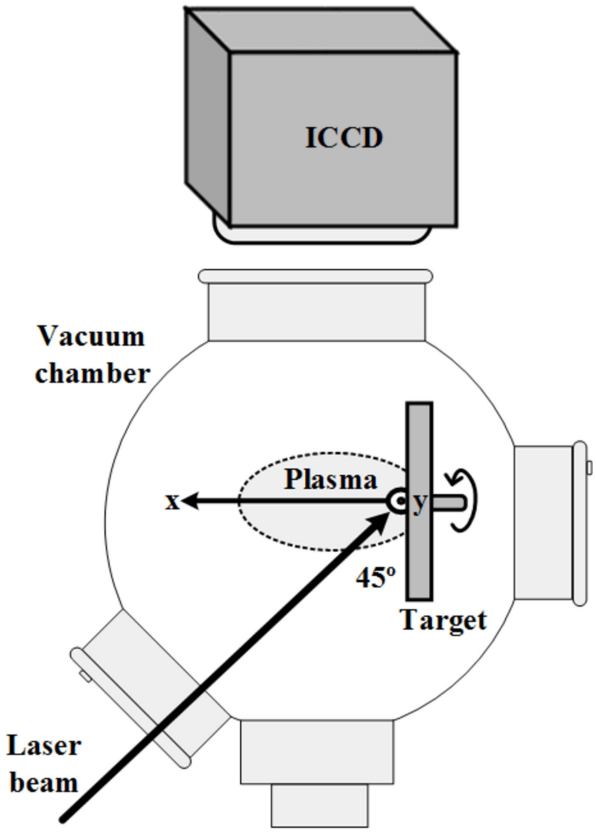

FIGURE 1. Schematic representation of the laser ablation experimental set-up used for the experiments. The ICCD images obtained by fast photography correspond to the XY plane.

The photographs were taken using an intensified charge-coupled device (ICCD) from Princeton Instruments, model PI-MAX:2 1024UV, equipped with a 1024×1024 pixel gray scale sensor; the system has an internal delay generator. The camera spectral sensitivity is in the range of 180-900 nm with maximum sensitivity at 550 nm. The camera is equipped with an AF-S Micro NIKKON 60 mm f/2.8G ED lens placed 25 cm from the "xy" plane (see Fig. 1). During the image acquisition process, the laser pulse signal is registered by a fast photodiode that delivers a trigger signal to the ICCD in such a way that each image of the plume is obtained from a single laser pulse. Both the signals of the photodiode and the ICCD camera are registered with a Tektronik 500 MHz digital phosphor oscilloscope, model TDS5054B. The ICCD gain was kept constant during image acquisition.

In order to study the laser ablation plumes, three sets of photographs were acquired. Each set consists of several series of photographs and each series corresponds to an Ar pressure value or vacuum. Table I shows the parameters used to take the photographs of each set. Each photograph series was acquired to characterize the plasma plume evolution under different background argon pressure [see Table II].

Hereafter, the time assigned to each photograph taken is the gate delay plus one half of the gate width. The photographs series of Set 1 were stored in 8-bit jpg format (gray-scale) and were processed using Matlab 7.9.0 (R2009b). The photographs of the Sets 2 and 3 were stored in 16-bit jpg format (gray-scale) and processed using WINSPEC (SPE).

2.2. Analysis methods used to study the ICCD images of the expanded laser ablation plume

Conventional analysis of the expanded plasma plume photographs was performed by plotting the position-versus-time curves of the expanding plume components. The plasma plume components on which we will focus our attention are the fast component, the plume expansion front, and the maximum intensity into the core of the plume, respectively. As described below, other procedures were also employed to analyze ICCD images. These complementary analysis methods were based on the examination of several parameters such as intensity per unit time of pixel exposure, mean exposure intensity per pixel per unit time for a photograph, integrated intensity, and cross correlation. Set 1 is made up of Series 1, 2, and 3, which were acquired for the evolution of the plasma plume in vacuum and in 0.347 and 0.694 Torr argon background pressures, respectively. These photograph series were used to study plume behavior and to assess the usefulness of cross correlation analyses carried out.

For analysis of the fast component and expansion front of the plume as well as cross correlation analysis corresponding

TABLE I. Parameters used to take the three studied sets of photographs.

Set	Target	NPS[a]	LPP[b] (μm/pixel)	IGD[c] (ns)	GDS[d] (ns)	IGW[e] (ns)	GWS[f] (ns)	NP[g]
1	$Ni_{50}Mn_{37}Sn_{13}$	3	54	100.0	15	2	1	252
2	$Ni_{50}Mn_{37}Sn_{13}$	10	54	102.5	15	15	0	259
3	Cu	6	52	102.5	15	15	0	259

[a]NPS is the number of photograph series taken for each set. Photograph series were acquired from the evolution of plasma plume under different background argon pressures [see Table II].

[b]LPP is the length per pixel. From this parameter the distance between two points in a photograph can be obtained.

[c]IGD is the initial ICCD gate delay. This is the delay from the onset of the plasma plume formation to the moment in which the first photograph of a series is taken.

[d]GDS is the ICCD gate delay step. It is the increase of gate delay.

[e]IGW is the initial ICCD gate width. It is the starting exposure time.

[f]GWS is the ICCD gate width step. It is the increment of the gate width.

[g]NP is the number of photographs per series.

TABLE II. Background argon pressure values for the 3 sets of photographs recorded.

Ar pressure for Set 1 (Torr)	Ar pressure for Set 2 (Torr)	Ar pressure for Set 3 (Torr)
10^{-5a}	10^{-5}	0.043
0.347[b]	0.043	0.087
0.694[c]	0.087	0.130
	0.130	0.174
	0.174	0.260
	0.260	0.347
	0.347	
	0.434	
	0.607	
	0.694	

[a,b,c] These series of photographs are referred in the text to as Series 1, 2, and 3, respectively.

to Set 1, the intensity per unit time of exposure for a position located at the pixel coordinates (x, y), is defined as $I\Delta t_{x,y}$. Here we call intensity to the readout values of the pixels of a photograph, which is referred to the amount of the light captured by the ICCD. For a pixel in photograph j from Set 1, $I\Delta t_{x,y}$ is given by:

$$\mathrm{I}\Delta t_{x,y,j} = (\mathrm{I}_{x,y,j} - \mathrm{Im}bj)/\Delta t_j. \tag{1}$$

Where $I_{x,y,j}$ is the intensity of a pixel located at the (x, y) coordinates of photograph j, Δt_j the exposure time (gate width) for photograph j, and $\mathrm{Im}b_j$ the mean intensity per pixel of the background emission for photograph j. To calculate $\mathrm{Im}b_j$ for a given pixel, a photograph of the zone studied is taken prior to initiating the ablation process. $\mathrm{Im}b_j$ is given by:

$$\mathrm{Im}b_j = \frac{\sum_{x=1}^{n}\sum_{y=1}^{m}\mathrm{I}_{x,y,j}}{n \times m} \tag{2}$$

Where $n \times m$ are the dimensions in terms of pixels of the explored photographs. To get the intensity per unit time of exposure vs time curve corresponding to a pixel, the pixel coordinates (x, y) in the photographs of a series for the Set 1 were fixed. Then the intensity per unit time of exposure of each pixel for every photograph of a series was plotted. The number of pixels for the photographs of Set 1 was 1024×1024, so this is also the number of curves obtained for each photograph series.

In order to carry out the cross correlation, we proceeded as follows. For each photograph series of Set 1, the 1024×1024 intensity per unit time of exposure vs time curves was obtained. Then, comparing the curves obtained for the same pixel in two different photograph series, a cross-correlation coefficient was calculated. Each photograph series of Set1 was a collection of 252 photographs in which a photograph was represented by a 1024×1024 matrix. The intensity value of each pixel in a photograph was represented by $\mathrm{I}\Delta t_{a,x,y,j}$ (*i.e.* each element of the matrix), where $\mathrm{I}\Delta t$ is the intensity per unit time of exposure, a is the number of the correlated series, (x, y) are the row and column of the photograph matrix and j is the photograph number (different photograph numbers imply a different time), respectively. So, keeping the value of a and the pixel coordinates (x, y) constant intensity per unit time of exposure vs time curve was obtained. As an example, the cross-correlation coefficient r of the corresponding curves for the pixel with coordinates (777, 477) located at 0.90 cm from the target surface (see Fig. 3) in Series 1 and 2 photographs ($r_{(777,477),1,2}$) was computed using the equation:

$$r_{(777,477),1,2} = \frac{\sum_{j=1}^{252}\mathrm{I}\Delta t_{1,777,477,j}\mathrm{I}\Delta t_{2,777,477,j}}{\left[\sum_{j=1}^{252}\left(\mathrm{I}\Delta t_{1,777,477,j}\right)^2\sum_{j=1}^{252}\left(\mathrm{I}\Delta t_{2,777,477,j}\right)^2\right]^{1/2}} \tag{3}$$

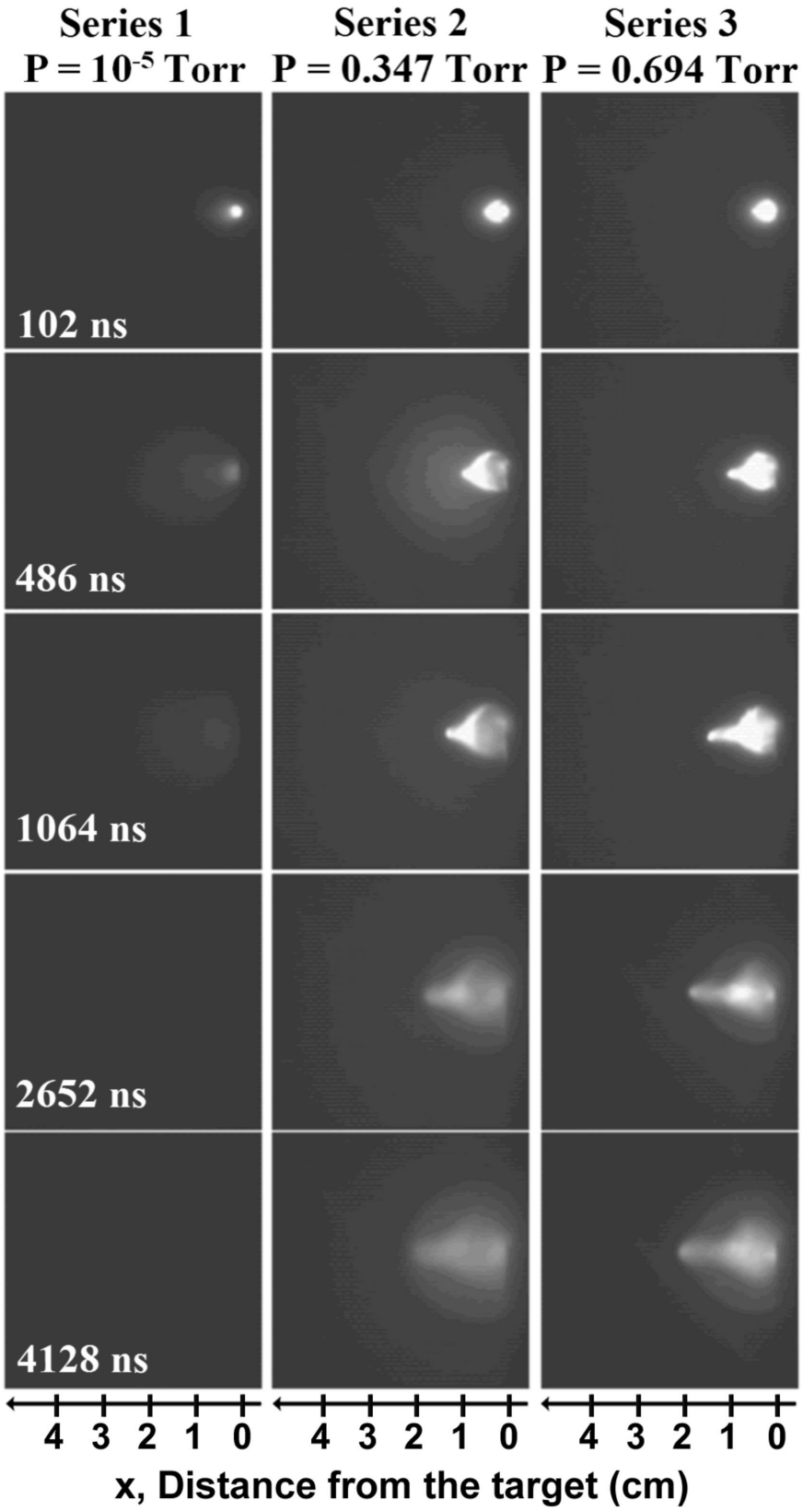

FIGURE 2. Temporal evolution of visible emission of the plasma plume generated by laser ablation of the $Ni_{50}Mn_{37}Sn_{13}$ target for Series 1, 2, and 3 recorded using an ICCD camera. The time indicated in the images is the time after the onset of the plasma formation. The horizontal axis at the bottom of each vertical set of photographs indicates the distance measured from the target surface.

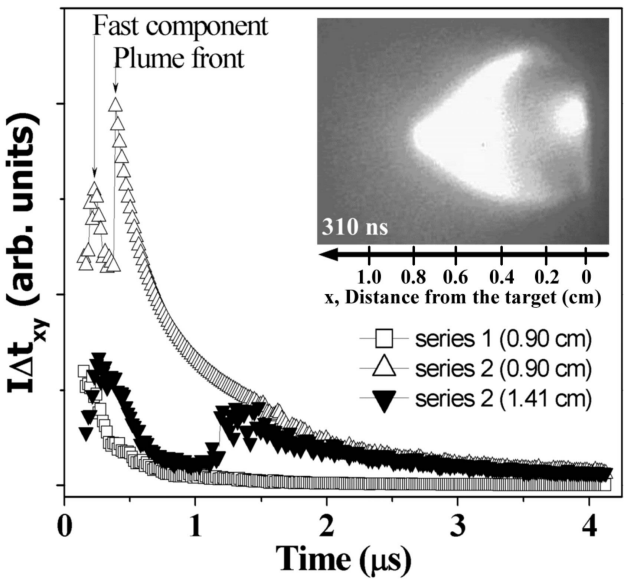

FIGURE 3. Intensity per unit time of exposure ($I\Delta t_{x,y}$) as a function of time for Series 1 (□) and 2 (Δ) in the position of lower cross-correlation coefficient ($r_{(777,477),1,2} = 0.744$) at 0.90 cm from the incidence point of laser pulse along the normal to the $Ni_{50}Mn_{37}Sn_{13}$ target surface [see Eq. (3)] and at 1.41 cm for the series 2 (▼). The vertical arrows indicate the fast component and the plume expansion front, respectively. Inset: ICCD image obtained at 310 ns for the series 2; the image clearly shows the plume expansion front and the slower moving/stationary component near the target surface.

Calculating the cross-correlation coefficients for all the 1024×1024 pixels, we obtained a gray-scale correlation photograph. The cross-correlation coefficient (r) varies between 0 and 1. When r is close to 1, both ablation plumes exhibit a similar intensity per unit time of exposure vs time curves; however, a value much lower than1 indicates they are quite different.

For the analysis of the sets 2 and 3, the mean intensity per pixel per unit time of exposure (I$p\Delta t$) for each photograph is defined by:

$$\mathrm{I}p\Delta t_j = \frac{\sum_{x=1}^{n}\sum_{y=1}^{m}(\mathrm{I}_{x,y,j} - \mathrm{I}mb_j)}{(n \times m)\,\Delta t_j}. \qquad (4)$$

where $\mathrm{I}_{x,y,j}$ is the intensity of a pixel located at the coordinates (x,y) in photograph j, $\mathrm{I}mb_j$ is the mean intensity per pixel of the background emission of photograph j [as defined by Eq. (2)], Δt_j is the exposure time. The dimensions in terms of the number of pixels ($n \times m$) of the photographs for the sets 2 and 3 were 392×501 and 451×601, respectively. From the mean intensity per pixel per unit time of exposure (I$p\Delta t$) for each photograph of a series, the mean intensity per pixel per unit time of exposure vs. time curves can be obtained. Integrating these curves over time, the integrated intensity parameter as function of time was obtained.

3. Results and Discussions

Figure 2 shows the temporal evolution of the visible emission of the plasma plume generated by the laser ablation of the $Ni_{50}Mn_{37}Sn_{13}$ target for Series 1, 2, and 3 recorded using an ICCD camera; they are representative photographs of Set 1. They were taken in vacuum (left vertical set), at 0.347 Torr (central vertical set) and at 0.694 Torr (right vertical set). The main differences between the laser ablated expansion plume obtained in vacuum and under a background argon atmosphere lie in the shape and the lifetime of visible zones. Notice that after approximately 1600 ns the light intensity in the photographs of Series 1 approached zero. However, the expansion of the plume in argon, compared to the one expanded in vacuum, showed a slower expansion rate with more luminous intensities. It can be considered that the plasma expansion into a vacuum is adiabatic [14,15].

It is known that the expansion of the laser ablation plume under intermediate background gas pressures involves the division of the plume into three components [2,3,11,12]. They are the fast component traveling at nearly the speed in vacuum [2] the plume expansion front, and the more slowly-moving/stationary component near the target surface [3,11,12] respectively. However, as far as we know the identification of the fast component using the fast photograph analysis has not been previously reported [2,3] Hariral *et al.* [2] suggested the use of space and time resolved spectral emission as a complementary way to identify the fast component.

Amoruso *et al.* [3] did not observe a significant signal from the fast component in their fast imaging analysis. This result was attributed to (i) the lower emission of the fast component, which is characterized by a lower density and a little interaction with the background gas; (ii) the limited dynamic range of the ICCD camera, which does not allow the detection of the very faint emission of the fast species.

In contrast with previous works, in the present study the triple structure of the plasma has been obtained only by means of fast photography analysis. Figure 3 shows three functions of the intensity per unit time of exposure ($\mathrm{I}\Delta t_{x,y}$) as function of time for Series 1 and 2 in the position of lower cross-correlation coefficient ($r_{(777,477),1,2} = 0.744$) at a distance of 0.90 cm from the incidence point of laser pulse along the normal to the target surface [see Eq. (3)] and at 1.41 cm for the series 2. It must be noticed that the intensity per unit time of exposure ($\mathrm{I}\Delta t_{x,y}$) vs time curves can be used to identify the fast component and the plume expansion front, as Fig. 3 shows for the case of the expanding $Ni_{50}Mn_{37}Sn_{13}$ plasma into background argon pressure of 0.347 Torr (series 2). These two peaks in the $\mathrm{I}\Delta t_{x,y}$ vs. time curves, corresponding to both the fast component and the plume expansion front, can be viewed at the same time only for a distance interval between 0.79 and 1.66 cm from the target position. Shown in the inset of Fig. 3 is an ICCD image taken during the evolution of the ablation process corresponding to the instant time of 310 ns for the series 2; notice that two luminous zones appear: the plume expansion front and the slower

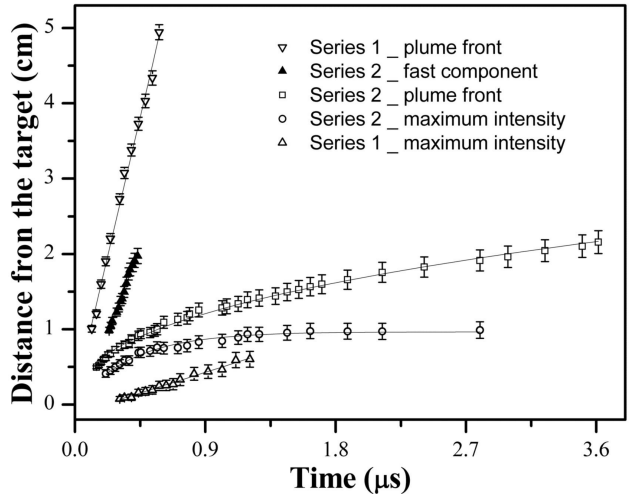

FIGURE 4. Position vs. time curves for Set 1 ($Ni_{50}Mn_{37}Sn_{13}$ target): the expanded plasma plume front in vacuum (∇), and at a background argon pressures of 0.347 Torr ($\square$), the maximum intensity in the core of the expanded plume in vacuum (Δ) and at a background argon pressure of 0.347 Torr ($\bigcirc$), and the fast component at 0.347 Torr ($\blacktriangle$). Continuous lines represent the calculated fits using equations 5 and 6.

moving/stationary component near to the target surface. It should be noticed that these two latter components may be clearly seen separately only in a time interval between 230 and 390 ns.

The fast photography analysis has been ordinarily used to plot the position of the luminous plume expansion front and the maximum intensity in the core of the plume as a function of time [2,3,16]. Frequently, the luminous expansion front is roughly located on the photographs with the naked eye [16,17] or considering a relative percentage of the maximum luminous intensity [18]. Figure 4 shows the position vs. time curves for the $Ni_{50}Mn_{37}Sn_{13}$ plume expansion front and the maximum intensity in the plume expanded in vacuum at a background argon pressure of 0.347 Torr (series 1 and 2). In this figure the luminous expansion front has been located on the photographs with both the aid of the naked eye and the use of intensity per unit time of exposure ($I\Delta t_{x,y}$) vs time curves. In order to identify the maximum intensity into the plume core cuts of the plume emission along the normal to the target surface on the photographs were used. The corresponding position vs. time curve of the plume fast component at a background argon pressure of 0.347 Torr, was also plotted. The continuous lines in the figure were the calculated fits obtained using Eqs. 5 and 6.

From the analysis of Fig. 4, a mean velocity of 5.32 ± 0.14 cm/μs was estimated for the fast component of the expanding plume at a background argon pressure. As expected, this value was lower than the velocity of the expanding plume front in vacuum (8.24 ± 0.19 cm/μs). The mean velocity of the maximum intensity in the core of the plume expanded in vacuum, *i.e.* 0.61 ± 0.02 cm/μs, was also lower. To study the plume expansion front and the maximum intensity in the core of the plume into argon, we used the shock wave and drag models, respectively [16]. We found that the data collected for the plume expansion fit very well within a shock wave model to the one corresponding to the plume expansion front. On the other hand, the drag model provides a better fit for the data corrected for the maximum intensity around the core of the plume. Similar results for the fit of the plume expansion front and the maximum intensity had been previously reported [18]. The shock wave model equation used was as follows [19]:

$$d = ct^n \,. \tag{5}$$

where c is a parameter that depends on the energy of the laser pulse, the density and the heat capacity of the background gas, and the exponent n is 0.4 for an ideal spherical shock wave [20]. In the present case we obtained the values $c = 1.26 \pm 0.01$ cm/μs$^{0.42}$ and $n = 0.42 \pm 0.01$.

In order to fit the shift of the maximum intensity in the core of the plume expanding into a 0.347 Torr background argon pressure the following equation for the drag model was applied :

$$d = d_{st}\,(1 - \exp(-\beta t))\,. \tag{6}$$

where d_{st} is referred to as the stop distance or the distance at which according to the model this plasma component is expected to stop and, β is the slowing coefficient. The values obtained from the fitting were: $d_{st} = 0.97 \pm 0.01$ cm and $\beta = 2.55 \pm 0.09$ μs^{-1}.

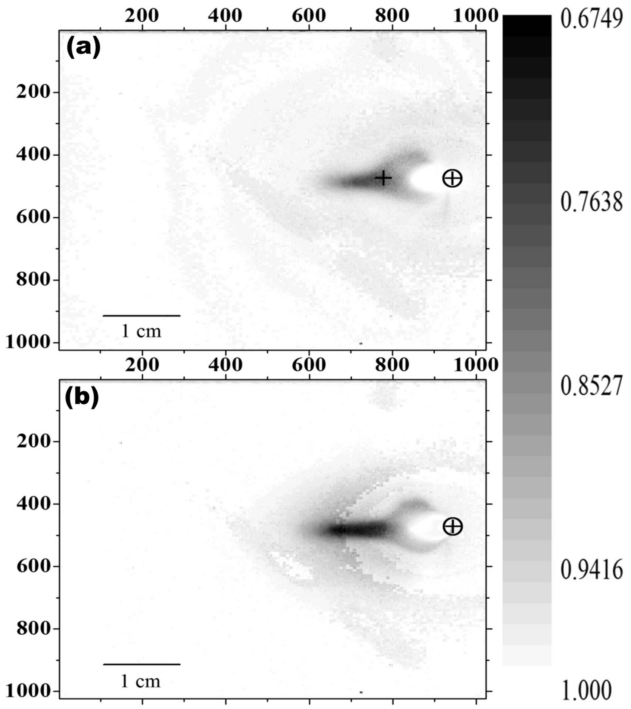

FIGURE 5. Correlation photographs for Series 1 and 2(a) and Series 1 and 3(b). The crossed symbol $\oplus$ indicates the incidence point of the laser pulse on the target surface. In (a) the crossed symbol + indicates the coordinates (777,477) for which the minimum cross-correlation coefficient is found, using the curves shown in Fig. 3.

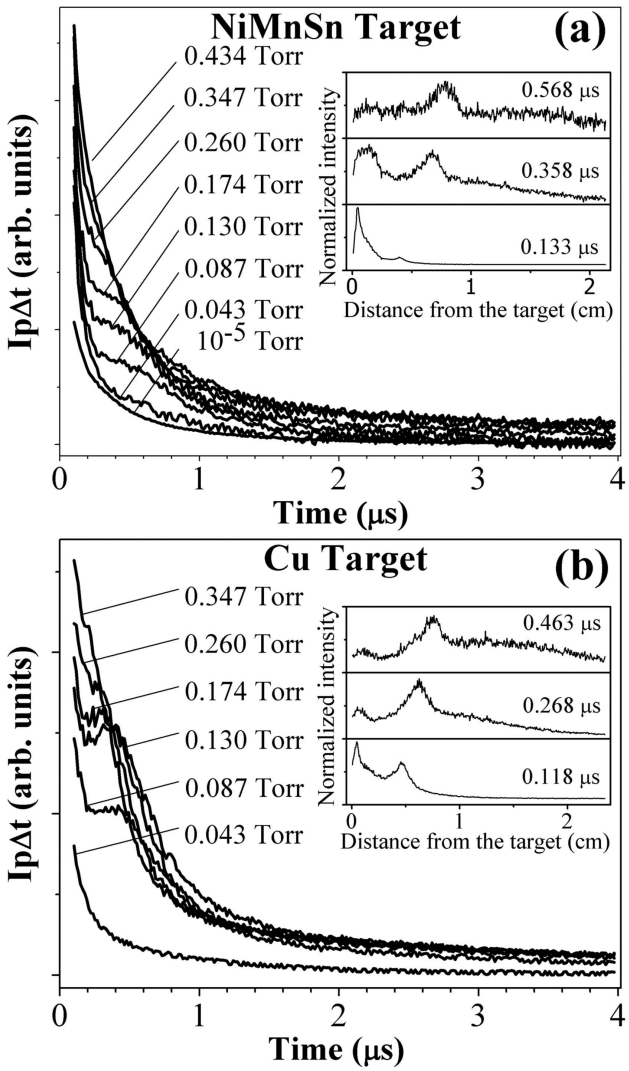

FIGURE 6. Curves of the mean intensity per pixel per unit time of exposure (I$p\Delta t$) as a function of time for the photograph series corresponding to Set 2 (a) and 3 (b). In (a), the I$p\Delta t$ as a function of time curves corresponding to argon background pressures of 0.607 and 0.694 Torr are not presented because the curves almost overlap with the curve obtained for 0.434 Torr. The insets in both figures show cuts of the plasma emission at three different times for the plasmas expanded at a background argon pressure of 0.174 Torr.

The curves of intensity per unit time of exposure (I$\Delta t_{x,y}$) as function of time were used to compare two different series of photographs. They were useful in finding the similarities and differences between the 3 photograph series of Set 1. Figure 3 shows the intensity per unit time of exposure (I$\Delta t_{x,y}$) as function of time for the pixel coordinates (777,477), located at 0.90 cm from the surface of the $Ni_{50}Mn_{37}Sn_{13}$ target, for the expanded plasma plume in vacuum (Series 1), and at background argon pressure of 0.347 Torr (series 2). The lower cross-correlation coefficient r between Series 1 and 2, which is given by Eq. (3), was found for these curves. We realized that the low cross-correlation coefficient between the two curves is due to the split of the expanding laser ablation plume into the background atmosphere (*i.e.* the fast component and the plume expansion front). From the 1024×1024 cross-correlation coefficients, the correlations photographs shown in Fig. 5 were constructed. Figure 5(a) displays the correlation photograph for Series 1 and 2. The symbol + in this figure indicates the pixel coordinates (777,477), located at 0.90 cm from the incidence point of laser pulse along the normal to the $Ni_{50}Mn_{37}Sn_{13}$ target surface. This is the position of lower cross-correlation coefficient ($r_{(777,477),1,2} = 0.744$). This coefficient was obtained using the curves shown in Fig. 3. Figure 5(b) is the correlation photograph for Series 1 and 3. They are quite similar. The crossed symbol $\oplus$ in the figures indicates the incidence point of the laser pulse on the target surface. In our correlation photographs the lower cross-correlation coefficient obtained was 0.6749. The latter was obtained from the correlation between Series 1 and 3 photographs at pixel coordinates (688,486). In our gray-scale correlation photographs, the cross-correlation coefficients scale varied from 0.6749 to 1. Figures 5(a) and (b) show an area near the target position for which high cross-correlation coefficients were obtained. This behavior corresponds to the fact that the early stages of the expansion of the plume in vacuum are similar to the ones obtained in intermediate background gas pressures [21]

In this area, near the target surface, the intensity per unit time of exposure vs time curves decreased monotonically. The areas with lower cross-correlation coefficients coincide with those where the fast component and the plume expansion front were observed through the analysis of the Series 2 and 3 photographs.

Figure 6 shows the mean intensity per pixel per unit time of exposure I$p\Delta t$ as a function of time curves [calculated using Eq. (4)] for Sets 2 and 3 photograph series. As shown in Fig. 6(a), this magnitude displays a monotonous decrease in both vacuum and at a background argon pressure of 0.043 Torr. This should be a consequence of similar behavior exhibited by expansion of the plume in vacuum and at low background pressures [2] Also notice that the curve corresponding to the expanded Cu plume at a background argon pressure of 0.043 Torr shown in Fig. 6(b) shows a monotonous decreasing behavior.

As Fig. 6 shows, in the background argon pressure range between 0.087 and 0.347 Torr the monotonous decreasing behavior of $Ip\Delta t$ as a function of time curves exhibited some variations below 1.0 μs, which depend on the background argon pressure. The photographs in this time interval show that the emission profiles of the plume split into two components: the plume expansion front and the more slowly moving/stationary component near the target surface. Considering the two curves obtained at a background argon pressure of 0.174 Torr as examples, the inset of each graph in Fig. 6 shows cuts of the plume emission along the normal to the target surface at three different time intervals of the emission process: before (at 0.133 μs and 0.118 μs, respectively), in (at 0.358 μs and 0.268 μs, respectively) and after (at 0.568 μs and 0.436 μs, respectively) the time interval at which the monotonous decrease behavior of I$p\Delta t$ is altered

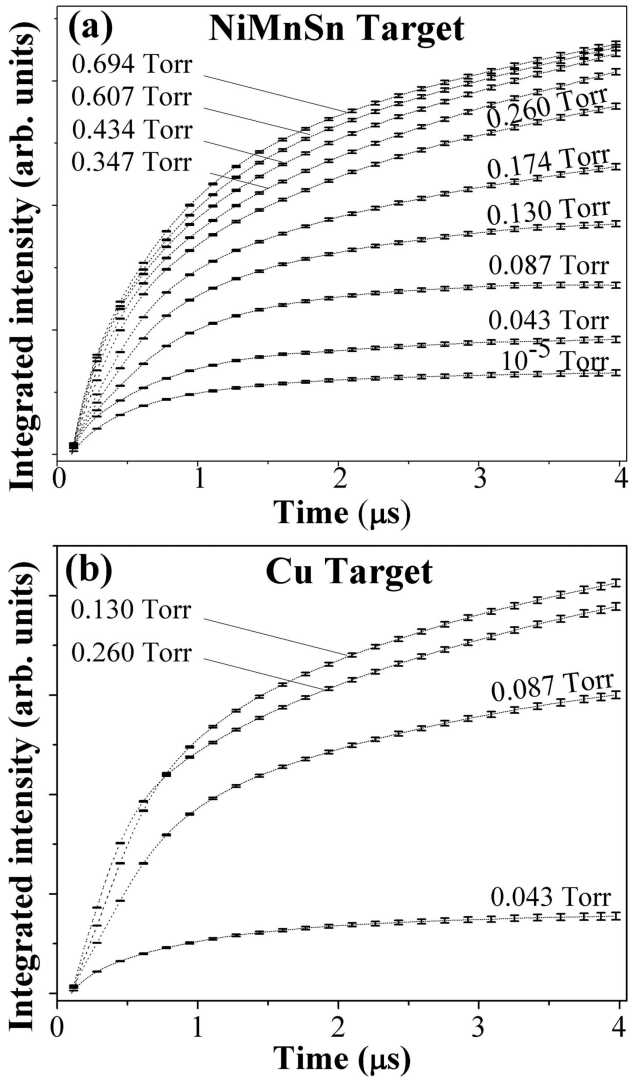

FIGURE 7. Integrated intensity as a function of time curves for the photograph series corresponding to the sets 2 (a) and 3 (b). In (b), the integrated intensity as a function of time curves corresponding to background argon pressures of 0.174 and 0.347 Torr are not presented because these curves almost overlap with the curve corresponding to 0.260 Torr.

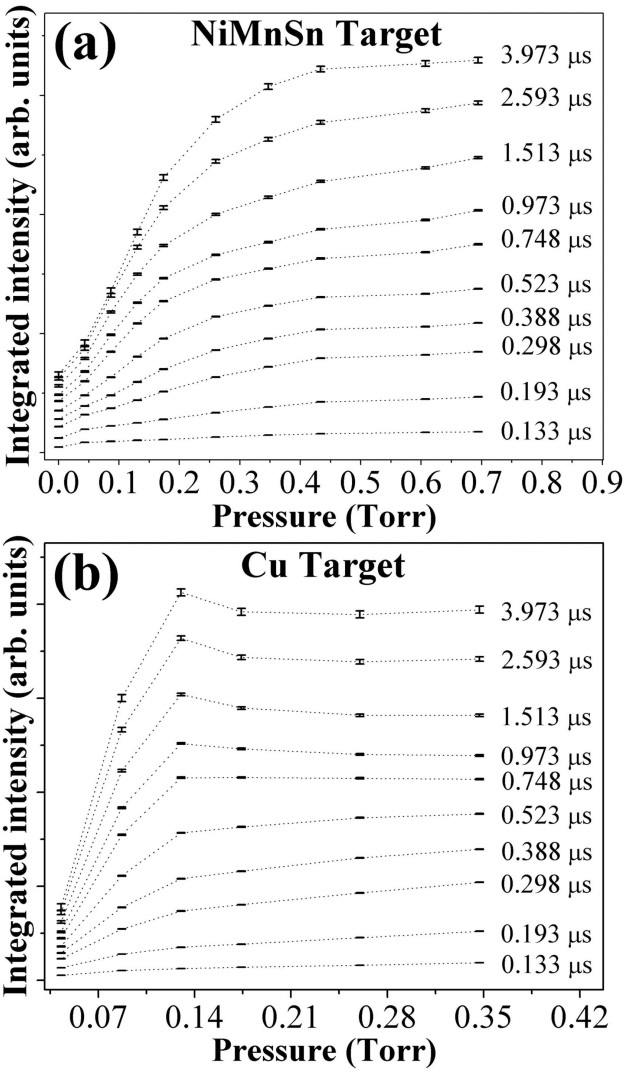

FIGURE 8. Integrated intensity as a function of pressure curves for the photograph series corresponding to Sets 2 (a) and 3 (b).

for $Ni_{50}Mn_{37}Sn_{13}$ (set 2) and Cu (set 3) plasmas, respectively. For early times, *i.e.* at 0.133 μs and at 0.118 μs in the insets of Fig. 6(a) and (b), respectively, the plume expansion front was forming and therefore the component close to the target surface became the higher intensity component. For moment of times in the middle of the time interval *i.e.* where the variation of the monotonous decrease behavior is observed (as the insets show at 0.358 μs and 0.268 μs), the plume expansion front was formed becoming the higher intensity component. For largest times (at 0.568 μs and 0.463 μs in the insets), splitting was absent and again $Ip\Delta t$ decreases monotonically. The previously mentioned time intervals, where the plume expansion front and the more slowly moving/stationary component near the target surface can be observed separately (*i.e.* the plasma splits), were reduced and their extreme values shifted toward early times as the argon pressure increased. According to Mahmood *et al.* [12] these facts may be explained considering that pressure increment results in the slowing down of the plume front due to a high degree of interaction of the plume species with the background gas. This interaction results in the diffusion of the more slowly moving/stationary component near the target surface into the background gas atmosphere. According to Amoruso *et al.* [3] the splitting occurs during the formation of the plasma plume-background gas contact front but before a significant braking of the plume expansion takes place. Then the plume species, which are scattered in a backward direction due to their collisions with the background gas molecules, interact with the incoming particles and after a while the plume homogenizes. For an argon background pressure higher than 0.434 Torr, a monotonic decreasing in I$p\Delta t$ as a function of time curves was observed. In these cases two simultaneous phenomena were observed: a fast deceleration of the plume expansion front and its coa-

lescence with the more slowly moving/stationary component.

Figure 7 shows the integrated intensity as a function of time curves for different background argon pressures for the photograph series corresponding to Sets 2 (a) and 3 (b). They were obtained by integrating in time the curves plotted in Fig. 6. The integrated intensity value in every moment corresponds to the amount of light captured by the ICCD camera from the starting time of the analysis until that moment.

All the curves of the integrated intensity as a function of time exhibit a similar behavior. For early times of the plume expansion process, the integrated intensity monotonically increases. However, the rate of increase decreases as time passes. As Fig. 7(a) shows, for the $Ni_{50}Mn_{37}Sn_{13}$ plasma plume, the curves of integrated intensity as a function of time approach one to another as the background argon pressure increases; thus at every moment an integrated intensity saturation value was reached. In the case of the Cu plume Fig. 7(b) shows that there are intersections of the curve corresponding to 0.130 Torr with those corresponding to 0.174, 0.260 and 0.347 Torr. These crossings can be explained by Fig. 8 where the integrated intensity is represented as function of pressure for different moments. It must be noted that there are pressure ranges in which the integrated intensity changes. These pressure ranges were from vacuum up to a background argon pressure of 0.434 Torr for the $Ni_{50}Mn_{37}Sn_{13}$ and from vacuum up to a background argon pressure of 0.174 Torr for the Cu plasma plumes, respectively. In general in these pressure ranges an increase in the integrated intensity is observed. In the case of Cu plasma plume this increase is not monotonous; in this case, there is an intermediate pressure value ($\sim$ 0.130 Torr) for which a maximum integrated intensity value is reached explaining the intersections between the curves in Fig. 7(b). For higher pressures saturation values of the integrated intensities were obtained within the pressure range considered in the present study. Using the above-proposed methods and parameters we have not found solid evidences of differences in the plasma plume behavior that could be attributed to the composition of the target. It is necessary to take into account that frequently the differences in the evolution of distinct species of the plume are optically related with the differences of the wavelengths emitted by these elements and in our experiments a gray scale ICCD camera was used.

4. Conclusions

In this work expanded use of the fast photography technique was applied to characterize laser-induced plasmas created from two different targets expanded in different background argon pressures: a multicomponent target of nominal composition $Ni_{50}Mn_{37}Sn_{13}$ and a target of highly pure Cu. By means of this technique it has been possible to find similarities and differences between two photograph series as well as to study the light emission as a function of time. With such a purpose some parameters, such as the intensity per unit time of exposure for a pixel, the mean intensity per pixel per unit time of exposure for a photograph, the integrated intensity and the cross correlation, were used. Both the intensity per unit time of exposure as a function of time curves and the cuts of the plume profile along the normal to the target surface enabled us to study the triple structure of the plasma plume (*i.e.* the plume expansion front, the maximum intensity in the core of the plume and the fast component traveling at a speed close to the speed in vacuum) expanding into an argon background. In contrast with previous studies, these results were obtained only by analyzing the ICCD fast photography images. The correlation photographs enabled the identification of plume zones with high and low cross-correlation coefficients, which are related to similarities and differences between $Ni_{50}Mn_{37}Sn_{13}$ plasma plumes expanding in vacuum and into argon background pressures. The mean intensity per pixel per unit time of exposure can be used as a measurement of the amount of light emitted by the plume at a given moment and can be represented as a function of time. For plasma plumes expanded in vacuum and at low background argon pressures (*i.e.* in the case of free expansion), the amount of light emitted decreases monotonically over time. For the plasma plume expanding into intermediate background argon pressures, the monotonic decreasing behavior is changed in the time interval in which the plasma plume splitting exists. From the analysis of the integrated intensity, as a measure of the total amount of light emitted until a given moment, two different pressure ranges were identified: one in which the integrated intensity is mainly increasing its value and another in which this magnitude becomes saturated. The proposed methods should be taken as a complement to the existing techniques and not as a substitution of them.

Acknowledgments

The authors acknowledge financial support received from: (a) CONACYT, Mexico, under projects CB 176705, CB-2010-01-157541 and CB183728; (b) from ICyTDF, UACM, Gobierno del Distrito Federal-Mexico and Laboratorio Nacional de Investigaciones en Nanociencias y Nanotecnología (LINAN, IPICYT); (c) from DGAPA, UNAM, under project IN 112112. The authors acknowledge José Castro for technical support.

1. S. George, A. Kumar, R. K. Singh, and V. P. N. Nampoori, *Appl. Phys. Lett.* **94** (2009) 141501.
2. S. S. Harilal, C. V. Bindhu, M. S. Tillack, F. Najmabadi, and A. C. Gaeris, *J. Appl. Phys.* **93** (2003) 2380.
3. S. Amoruso, A. Sambri, M. Vitiello, and X. Wang, *Appl. Surf. Sci.* **252** (2006) 4712.
4. A. K. Sharma and R. K. Thareja, *Appl. Phys. Lett.* **84** (2004) 4490.
5. S. Abdelli-Messaci, T. Kerdja, S. Lafane, and S. Malek, *Part B* **64** (2009) 968.
6. A. Misra and R. K. Thareja, *IEEE Trans. Plasma Sci.* **27** (1999) 1553.
7. S. Lafane, T. Kerdja, S. Abdelli-Messaci, S. Malek, and M. Maaza, *Appl. Phys. A* **98** (2010) 375.
8. D. B. Geohegan and A. A. Puretzky, *Appl. Phys. Lett.* **67** (1995) 197.
9. H. Haberland, Z. Insepov, and M. Moseler, *Phys. Rev. B* **51** (1995) 11061.
10. C. N. Afonso *et al*., *Appl. Phys. A* **69** (1999) S201.
11. R. K. Thareja, A. Misra, and S. R. Franklin, *Spectrochim. Acta, Part B* **53** (1998) 1919.
12. S. Mahmood, R. S. Rawat, M. S. B. Darby, M. Zakaullah, S. V. Springham, T. L. Tan, and P. Lee, *Phys. Plasmas* **17** (2010) 103105.
13. E. de Posada, M. A. Arronte, L. Ponce, E. Rodríguez, T. Flores, and J. G. Lunney, *Journal of Physics: Conference Series* **274** (2011) 012078.
14. S. I. Anisimov, D. Bäuerle, and B. S. Luk'Yanchuk, *Phys. Rev. B* **48** (1993) 12076.
15. C. L. Liu, J. N. Leboeuf, R. F. Wood, D. B. Geobegan, J. M. Donato, K. R. Chen, and A. A. Puretzky, *Mater. Sci. Eng. B* **47** (1997) 70.
16. D. B. Geohegan, *Applied Physics Letters* **60** (1992) 2732.
17. A. Misra, A. Mitra, and R. Thareja, *Applied Physics Letters* **74** (1999) 929.
18. C. Phelps, C. J. Druffner, G. P. Perram, and R. R. Biggers, *J. Phys. D* **40** (2007) 4447.
19. B. Angleraud, C. Girault, C. Champeaux, F. Garrelie, C. Germain, and A. Catherinot, *Appl. Surf. Sci.* **96** (1996) 117.
20. S. H. Jeong, R. Greif, and R. E. Russo, *J. Phys. D* **32** (1999) 2578.
21. S. Amoruso, J. Schou, and J. G. Lunney, *Appl. Phys. A* **92** (2008) 907.